Z. Phys. B – Condensed Matter 77, 185–191 (1989)

Condensed Matter
Zeitschrift für Physik B

Magnetic properties and antiferromagnetic Cu ordering in Pr_2CuO_4

P. Allenspach[1], S.-W. Cheong[2], A. Dommann[3], P. Fischer[1], Z. Fisk[2], A. Furrer[1], H.R. Ott[3,4], and B. Rupp[4,*]

[1] Labor für Neutronenstreuung, Eidgenössische Technische Hochschule Zürich, Villigen, Switzerland
[2] Los Alamos National Laboratory, Los Alamos, New Mexico, USA
[3] Laboratorium für Festkörperphysik, ETH Hönggerberg, Zürich, Switzerland
[4] Paul Scherrer Institut, Labor für Festkörperforschung, Villigen, Switzerland

Received May 22, 1989; revised version July 6, 1989

Bulk-magnetisation measurements and neutron-scattering experiments were performed both on a polycrystalline sample and on a single-crystal of Pr_2CuO_4 in the temperature range from 1.5 to 300 K. Pr_2CuO_4 crystallizes with the T' (Nd_2CuO_4)-type structure. We observed antiferromagnetic ordering of the Cu moments below $T_N=(190\pm2)$ K in a single crystal and below $T_N=(250\pm10)$ K in powder material. The magnetic unit cell dimensions are $a_m=2a_0$, $c_m=c_0$; the Cu moments are oriented in the basal plane with a magnetic saturation moment of $\mu_{Cu}=(0.45\pm0.12)\,\mu_B$. Pr^{3+} does not order magnetically above 1.5 K due to its crystal-field induced singlet ground state as verified by inelastic neutron scattering.

1. Introduction

Compounds of the type R_2CuO_4 (R = Pr, Nd) crystallizing in the T'-type structure (Fig. 1) recently gained considerable interest due to claimed *n*-type (electron carrier) superconductivity with T_c above 20 K in substituted systems such as R–Ce–Sr–Cu–O [1, 2] and fluorine doped Nd_2CuO_4 [3]. As in the case of La_2CuO_4 and $La_{2-x}M_xCuO_4$ compounds (M = Sr, Ba) it seems essential to investigate the properties of the parent compounds R_2CuO_4 below room temperature, especially with respect to their structural and magnetic behaviour. Knowledge of the magnetic properties of the Cu ions is particularly important in view of possible differences in the electronic structure of La_2CuO_4- and Pr_2CuO_4-isotypic compounds resulting mainly from distinct differences in their crystal structures: the oxygen atom O(2), which occupies the edges of the unit cell (0, 0, $z\approx0.18$) in the tetragonal La_2CuO_4-type structure (undistorted K_2NiF_4-type)

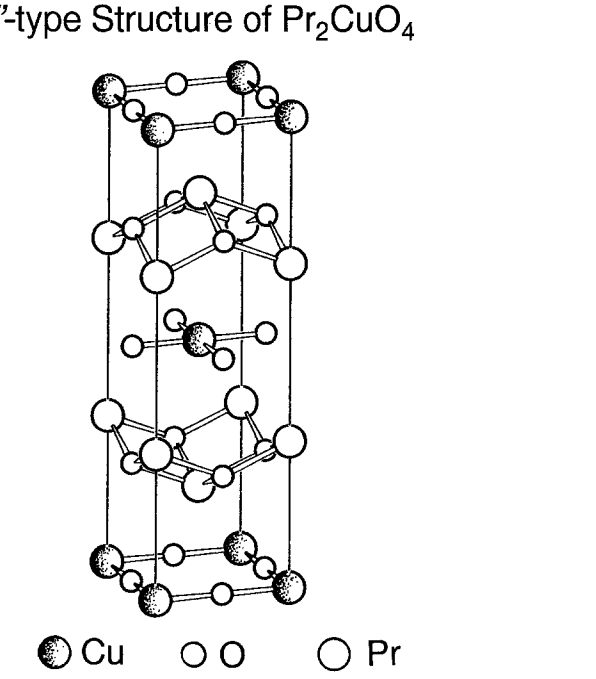

Fig. 1. T' (Nd_2CuO_4)-type crystal structure of Pr_2CuO_4. The bond sticks as choosen show the close relationship to the $BaAl_4$-type family of structures

* *Present address*: Lawrence Livermore National Laboratory, University of California, Livermore, CA 94550, USA

moves to the faces (1/2, 0, 1/4) of the Pr_2CuO_4 cell leading to a loss of the octahedral environment of Cu as it is found in La_2CuO_4, leaving a quadratic-planar CuO_2 arrangement in Pr_2CuO_4 (see eg. the reviews in [4, 5]; a further discussion follows in Sect. 3.2 of this paper).

In this work we report measurements of the macroscopic and microscopic magnetisation on Pr_2CuO_4 as well as a study of inelastic neutron scattering to probe the excitation within the crystal-field split ground-state multiplet of the Pr^{3+} ion. Both types of magnetisation measurements were done on single crystals while structural and additional crystal-field data were obtained from neutron scattering on a powder specimen. The present results reveal antiferromagnetic ordering of the Cu-moments in Pr_2CuO_4 below $T_N \approx 190$ K in the single crystal and $T_N \approx 250$ K in the powder material, similar in some details to what was observed in La_2CuO_4.

2. Experimental

Single-crystalline samples were prepared as described in Ref. 6; the powder sample was obtained from the respective oxides by a standard sintering technique and regrinding the material several times. The macroscopic magnetisation was measured using a moving-sample magnetometer between 1.5 K and room temperature and in external magnetic fields between 0 and 100 kOe, applied either parallel or perpendicular to the basal plane of the tetragonal T'-type unit cell. Neutron powder diffraction patterns with good profile statistics ($I_{max} > 50000$ counts) as required for the detection of very small magnetic superstructure reflections, were recorded at 20 K and at 293 K on the multidetector powder diffractometer DMC at the SAPHIR reactor of the Paul Scherrer Institute, Würenlingen, Switzerland (LN_2 cooled Si filter, vertically focussing $Ge_{(311)}$ monochromator, collimation 10′/-/12′, $\lambda = 1.7060(5)$ Å). The Pr_2CuO_4 powder was sealed under He in a cylindrical vanadium sample container of 10 mm diameter and 50 mm length. The diffraction patterns were refined by the Rietveld method using a modified code by Hewat [7]. Moreover, single-crystal neutron intensities were collected as a function of temperature on the 2-axis spectrometer P2AX($C_{(002)}$ monochromator, 60 mm pyrolytic graphite filter, $\lambda = 2.3340(5)$ Å) in ω-scan mode. Neutron scattering lengths were taken from Sears [8] and the magnetic form factor of Cu^{2+} was adopted from Akimitsu and Ito [9]. The samples were cooled down to 8 K using CTI closed-cycle helium refrigerators.

Inelastic neutron scattering (INS) experiments were performed on the triple-axis spectrometer IN2 (SAPHIR reactor, Würenlingen). The energy of the scattered neutrons was kept fixed at 13.7 meV giving rise to an energy resolution ($\Delta E = 0$) of 0.9 meV. To gain intensity, the measurements were carried out using a doubly-bent graphite monochromator as well as a horizontally-bent graphite analyzer, both with (002) scattering planes. Consequently, no collimations were used from neutron source to detector. A pyrolytic graphite filter was inserted into the outgoing neutron beam to reduce higher-order contamination. The experiments were performed for moduli of the scattering vector Q, temperatures and energy transfers in the ranges $1 \leqq \bar{Q} \leqq 6$ Å, $10 \leqq T \leqq 293$ K, and $0 \leqq \Delta E \leqq 110$ meV, respectively. A cylindrical Al sample container of 15 mm diameter and 50 mm length was used in the inelastic measurements.

3. Results and discussion

3.1. Powder diffraction and crystal structure

The neutron diffraction patterns recorded at room temperature and at 20 K, respectively, could be completely indexed using the tetragonal Pr_2CuO_4 cell (see Fig. 1) based on the Nd_2CuO_4 T'-type structure[5]. 59 nuclear reflections were refined in the centrosymmetric tetragonal space group $14/mmm$ (No. 139, D_{4h}^{17}) yielding nuclear agreement values R_1 concerning integrated intensities as low as 2% for both temperatures. With the exception of a very small reflection at $2\theta = 47$ deg, no additional peaks of impurity phases with contributions larger than 3 estimated standard deviations (e.s.d.'s) of background could be observed nor did we detect any signs for weak systematic superstructure reflections at room temperature. At 20 K, however, the powder spectra showed a tiny additional peak which could be indexed on the basis of an a-doubled tetragonal cell ($2a_0$, $2a_0$, c_0). The best fit for the nuclear refinement at 20 K is shown in Fig. 2; the additional (1/2, 1/2, 1)-peak is indicated by a marker. Table 1 includes structural, occupational and thermal parameters as well as agreement factors R_I for the room temperature and the 20 K refinements. The single free positional parameter $z_{(Pr)}$ is very similar to that of Nd_2CuO_4 [5]. Neither the nuclear neutron intensities nor additionally recorded low-temperature X-ray diffraction patterns (Cu K_α radiation) yield any indications for significant structural changes as observed in La_2CuO_4 between room temperature and 20 K.

3.2. Single-crystal studies of antiferromagnetic Cu ordering

A plate-like crystal fragment of $8 \times 10 \times 0.2$ mm (c-axis normal to the plate as verified by Mo K_α X-ray

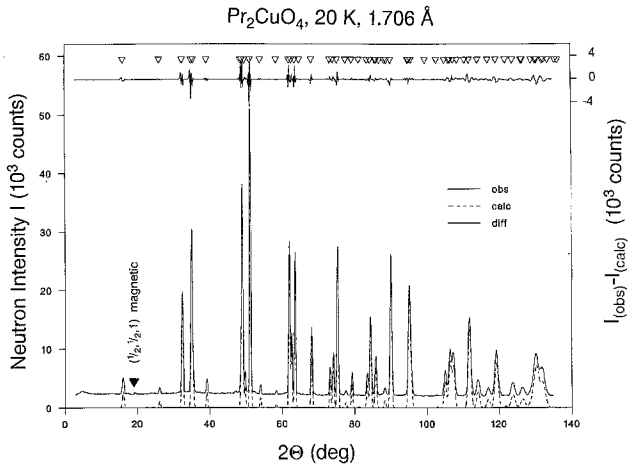

Fig. 2. Observed, calculated and difference neutron diffraction patterns of Pr_2CuO_4 at 20 K. Note the tiny magnetic ($^1/_2$, $^1/_2$, 1) reflection indicated by the marker

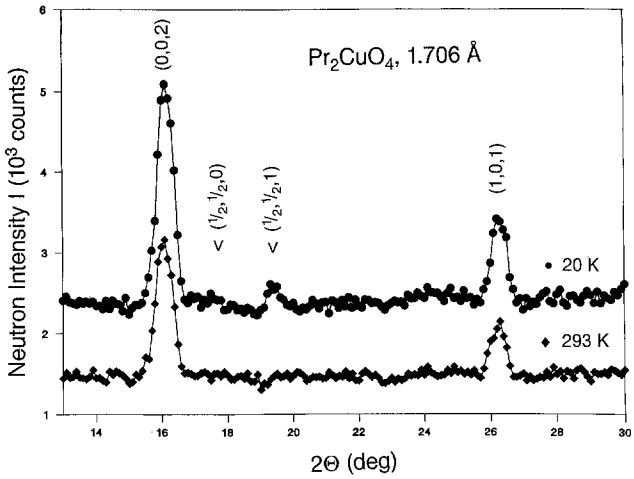

Fig. 3. Enlarged part of the Pr_2CuO_4 powder spectra recorded at 20 K and at 293 K. Note the zero intensity for ($^1/_2$,$^1/_2$, 0) and the disappearence of ($^1/_2$, $^1/_2$, 1) in the 293 K spectrum

Table 1. Structural parameters of Pr_2CuO_4, space group 14/mmm (No. 139, D_{4h}^{17}), $Z=2$. For refined parameters the numbers in parentheses give the e.s.d.'s of the last significant digit. Deviations from nominal composition (n) were in all cases and for all atoms less than 0.5% and therefore kept constant at their nominal values. For Pr, z is identical for 293 or 20 K as well. Reliability factors R were evaluated following the outlines of Young, Prince and Sparks [13]. R_I, R_{wp} are agreement values concerning integrated and weighted-profile intensities, respectively [7]. R_{exp} is the expected value based on counting statistics. Neutron wave length $\lambda=1.7060(5)$ Å, units for temperature factors B: Å^2

Atom	Site	x	y	z	n	$B_{(293\,K)}$	$B_{(20\,K)}$
Pr	4*e*	0	0	0.3515(2)	4.0	0.41(7)	0.21(7)
Cu	2*a*	0	0	0	2.0	0.35(5)	0.20(5)
O(1)	4*c*	0	1/2	0	4.0	0.69(5)	0.42(5)
O(2)	4*d*	0	1/2	1/4	4.0	0.59(5)	0.39(5)

Cell constants (Å) and R-values

T (K)	a_0	c_0	$R_{I(nuc)}$	R_{wp}	R_{exp}
293	3.9625(5)	12.2359(20)	2.14	8.18	2.59
20	3.9567(5)	12.1993(20)	2.16	8.15	1.96

precession photographs) was mounted on a copper sample holder on the two-axis spectrometer. The crystal orientations corresponded to directions [0, 0, 1] and [±1, ±1, 0] in the scattering plane. Rocking curves of the crystal revealed an imperfect mosaic distribution along the c-axis in contrast to (h, k, 0) reflections. Intensities of nuclear Bragg peaks were in good agreement with values calculated using the refined structural parameters from Table 1. Following the indications from the powder pattern, weak reflections (1/2, 1/2, 1) could be detected; the relative intensity of the largest observed additional peak (1/2, 1/2, 1) compared to strong nuclear peak intensities was below 1%. The absence of any additional peaks in low-temperature X-ray diagrams suggests an antiferromagnetic origin of the observed neutron single-crystal and powder reflections.

The observed magnetic peaks indicate the selection rules $h=2m+1$, $k=2n+1$ (n, m: integers) based on the magnetic unit cell with lattice constants $a_m=2a_0$, $c_m=c_0$. As the Cu^{2+} ions form a simple sublattice, this implies antiferromagnetic coupling along both [100] and [010]. From the absence of a magnetic peak (1, 1, 0) in both the 20 K neutron powder pattern (see Fig. 3) and in the case of 20 K single-crystal neutron intensities (see Table 2) the magnetic-moment directions $\pm[-1, 1, 0]$ or $\pm[1, 1, 0]$ may be derived (different domains corresponding to 90° rotation around the c-axis; reversal of moment direction does not change the neutron intensities). At these temperatures magnetic long-range order among the Pr moments can be excluded as well because of the singlet ground state of Pr^{3+} (see discussion of inelastic neutron scattering results below). Assuming magnetic moment direction $[-1, 1, 0]$ implies for a vanishing (1, 1, 0) peak furthermore ferromagnetic coupling between copper atoms at the center (1/4, 1/4, 1/2) of a chemical subcell and Cu at (0, 0, 0) and otherwise similar antiferromagnetic coupling at $z=0$ and $z=1/2$, respectively. A second possibility is moment direction [1, 1, 0] and antiferromagnetic coupling between Cu at (1/4, 1/4, 1/2) and (0, 0, 0). It corresponds to ferromagnetic (1, 1, 0) planes with antiferromagnetic coupling of adjacent planes of this type. This configuration differs from the first model shown in Fig. 4 only by a rotation of 90° around the c-axis, i.e. may be considered as an equivalent magnetic domain. Corre-

Table 2. Observed and calculated integrated magnetic neutron intensities (M) of Pr_2CuO_4 and weak nuclear intensities (considered to be free from extinction effects) used for scaling (N). In case of powder data the Cu moment was directly calculated from the magnetic peaks, whereas in the single-crystal case the moment was obtained by minimizing the differences in weighted intensities according to the reliability value $R_{Iw_{(mag)}}$ defined below. Temperature: 20 K

Powder data

	h	k	l	$I_{(obs)}(\sigma)$	$\lvert F\rvert^2_{(obs)}$	$\lvert F\rvert^2_{(cal)}$	$\mu_{(obs)}(\sigma)$
N	0	0	2	1715 (111)	17.28	16.8	–
N	1	0	1	575 (50)	4.0	3,9	–
M	$^1/_2$	$^1/_2$	0	0	0	0	–
M	$^1/_2$	$^1/_2$	1	147 (30)	1.05	1.05	0.49 (17)
M	$^1/_2$	$^1/_2$	4	42 (26)	1.23	0.91	0.76 (56)

Single-crystal data

	h	k	l	$I_{(obs)}(\sigma)$	$I_{(cal)}$	$I_{(obs)}-I_{(cal)}$
N	0	0	2	11539 (46)	15316	−3777
N	1	1	0	23184 (87)	23854	−670
N	1	1	2	18502 (118)	15219	3283
N	1	1	$\bar{2}$	16384 (680)	15219	1163
M	$^1/_2$	$^1/_2$	0	15 (19)	0	−15
M	$^1/_2$	$^1/_2$	1	409 (17)	365	44
M	$^1/_2$	$^1/_2$	2	151 (14)	149	2
M	$^1/_2$	$^1/_2$	3	96 (24)	279	−183
M	$^1/_2$	$^1/_2$	4	353 (23)	177	176
M	$^1/_2$	$^1/_2$	5	189 (39)	183	6
M	$^1/_2$	$^1/_2$	$\bar{1}$	397 (25)	365	32
M	$^1/_2$	$^1/_2$	$\bar{2}$	147 (13)	149	−2
M	$^1/_2$	$^1/_2$	$\bar{3}$	71 (25)	279	−208
M	$^1/_2$	$^1/_2$	$\bar{4}$	279 (32)	177	102
M	$^1/_2$	$^1/_2$	$\bar{5}$	175 (37)	183	−8

$\mu_{Cu}=0.45\,(12)\,\mu_B$, $R_{Iw_{(mag)}}=37\%$, $R_{Iw_{(nuc)}}=22\%$,
$R_{Iw_{(mag,nuc)}}=[\Sigma w_j\,(I_{(obs)_j}-I_{(cal)_j})^2/\Sigma w_j I^2_{(obs)_j}]^{1/2}$
$w_j=1/\sigma_j^2$

sponding calculated (including contributions from both magnetic domains (1, 1, 0) and (−1, 1, 0)) and observed magnetic neutron intensities are summarized in Tables 1 and 2 for powder and single crystal data, respectively. In view of the very low magnetic peak intensities involved, the small size and imperfection of the plate-like shaped crystal and the neglect of absorption and extinction effects, the agreement between observed and calculated domain-averaged magnetic neutron intensities is acceptable (Table 2). The data from the powder spectrum and from the single-crystal measurement are compatible and a resulting copper moment of about 0.45(12) μ_B was derived. As in La_2CuO_4 [10], such a value for the ordered magnetic saturation moment is considerably reduced if compared with the expected value $gS\approx 1\,\mu_B$ of Cu^{2+}.

Temperature dependence of Cu sublattice ordering. From the temperature dependence of the magnetic

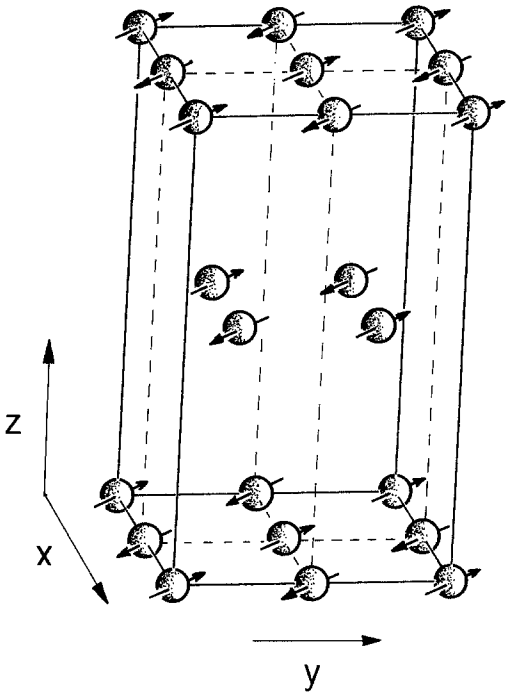

Fig. 4. The magnetic unit cell of Pr_2CuO_4

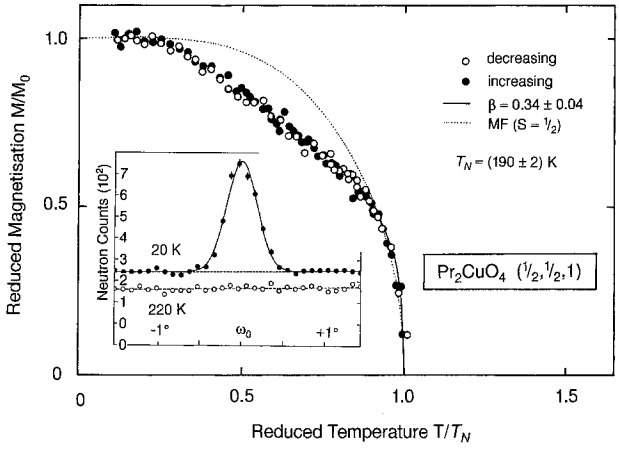

Fig. 5. Temperature dependence of the reduced sublattice magnetisation of Cu^{2+} in Pr_2CuO_4 as determined from neutron intensities of the single-crystal ($^1/_2$, $^1/_2$, 1) reflection. The dotted line represents a mean-field (MF) model for $S=^1/_2$, the solid line is a critical exponent fit ($C(1-T/T_N)^\beta$) yielding $\beta=0.34$ (4), $T_N=190$ (2) K. The inset shows the intensities of the ($^1/_2$, $^1/_2$, 1) reflection above and below T_N

(1/2, 1/2, 1) neutron peak intensity we obtained a reduced magnetisation curve as plotted in Fig. 5, which yields the Néel temperature $T_N=(190\pm 2)$ K. The inset of Fig. 5 shows single-crystal intensities of the magnetic peak (1/2, 1/2, 1) at 20 K and at 220 K, respectively. Also shown in Fig. 5 are a calculated mean-field ($S=1/2$) Brillouin curve as well as a critical expo-

nent fit ($C(1-T/T_N)^{\beta}$) of the initial slope of the magnetisation curve yielding $\beta=(0.34\pm0.04)$. Whereas from the value of the critical exponent β both a mean-field model and a 2-dimensional Ising model can be excluded, a distinction between the 3-dimensional models (Ising: $\beta=0.325$; 0.345; and Heisenberg: 0.365) is not unambiguously possible. A virtually identical characteristic shape of the temperature dependence was observed for the weaker magnetic single-crystal reflection (1/2, 1/2, 4). Taking into account the restriction of low counting statistics and a higher T_N of (250 ± 10) K, equivalent behaviour was found for the (1/2, 1/2, 1) reflection of the powder sample. The considerably enhanced ordering temperature $T_N=(250\pm10)$ K for the powder specimen could be the result of significant preparational differences between growing a single crystal from the flux melt compared to firing powder material in oxygen atmosphere: In the latter case it is reasonable to assume a maximum achievable oxygen content as in fact reflected by the full occupation of all oxygen sites (see Sect. 3.1) in the Pr_2CuO_4 structure. The single crystal may well contain some oxygen vacancies inducing probably a weakening of the Cu−O−Cu superexchange that would lead to a reduced T_N of 190 K in the single crystal. This strong dependence of T_N on oxygen concentration is analogous to what has been reported for La_2CuO_4 [10].

The temperature dependence of the sublattice magnetisation in Pr_2CuO_4 as shown in Fig. 5 deviates significantly from a spin-$\frac{1}{2}$ Brillouin function and is much better described by a temperature dependence claimed for 3-dimensional model systems. This is distinctly at variance from what is proposed for La_2CuO_4, which is essentially interpreted as a 2-dimensional, spin-$\frac{1}{2}$ Heisenberg system, where small corrections finally lead to 3-dimensional long-range ordering of the Cu^{2+} moments [10]. Some caution, however, is required when comparing model calculations with the magnetisation curve of Pr_2CuO_4. It cannot be excluded that the strange flattened shape of the magnetisation curve is the result of a superposition of subsequent different sublattice magnetisations, but as yet, there are no experimental evidences supporting such an assumption.

From a comparison between the crystal structures of Pr_2CuO_4 and of La_2CuO_4 it is not straightforward to conclude whether the 2-dimensional character of magnetism should be more or less pronounced in Pr_2CuO_4. Magnetic order in La_2CuO_4 occurs in the orthorhombically distorted version of the K_2NiF_4-type T structure while Pr_2CuO_4 keeps the original T' structure at all temperatures. The most obvious difference between these structures is the different oxygen-atom grouping around each copper atom. While in La_2CuO_4 an octahedral oxygen-cage surrounds each Cu atom and the octahedron's tilt in the orthorhombic La_2CuO_4 phase leads to a buckling of the Cu−O planes, the change in position of the O(2) atoms (forming the apexes of the oxygen octahedra in La_2CuO_4) leads to a loss of the octahedral environment in Pr_2CuO_4 and the Cu−O planes remain flat in the T' structure. As an additional result of the different position of the O(2) atoms it may be expected that the superexchange channel perpendicular to these planes is drastically altered in Pr_2CuO_4 compared to La_2CuO_4. Another obvious difference is the larger intraplane Cu−Cu distance in Pr_2CuO_4, which is, however, accompanied by a slight reduction of the distances between the planes when compared with corresponding atom separations in La_2CuO_4. The change of the superexchange geometry might weaken the interaction between the planes, but the reduction of the interplanar separation would on the other hand seem to favor 3-D behavior. In spite of those differences, the Néel temperatures for 3-dimensional long-range antiferromagnetic order are similar in both Pr_2CuO_4 and La_2CuO_4. The alignment of the ordered magnetic moments and their magnitude are again almost identical in both substances and one is tempted to interpret the results presented here with roughly the same arguments as those given in Ref. 10. Nevertheless, our observations of the temperature dependence of the Cu sublattice magnetization leave some doubt whether the magnetic properties of Pr_2CuO_4 are also essentially those of a two-dimensional system.

3.3. *Crystal-field studies*

Characteristic energy spectra obtained by INS are shown in Fig. 6. The scattering is dominated by an

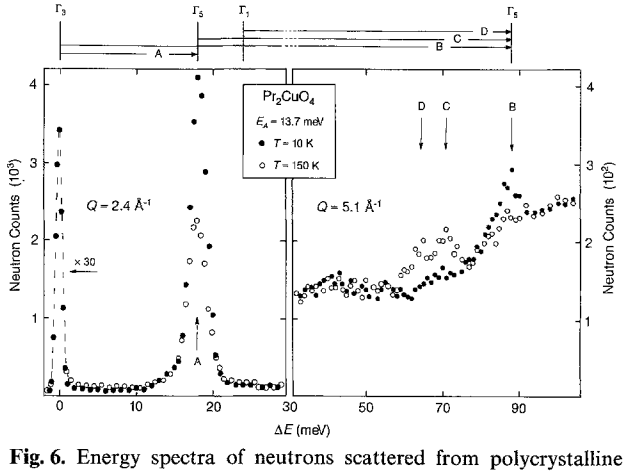

Fig. 6. Energy spectra of neutrons scattered from polycrystalline Pr_2CuO_4. The lower part of the resulting crystal-field level scheme is indicated on the top of the figure

intense inelastic line (peak A) at 18 meV whose intensity decreases upon raising the temperature; so it can immediately be interpreted as a ground-state crystal-field transition. The same is true for the much weaker line (peak B) at about 88 meV. Excited crystal-field transitions show up at about 68 meV (peaks C and D). We have confirmed the magnetic origin of all these lines by studying the peak intensities versus modulus of the scattering vector $\vec{Q}$ which exhibit the expected form factor behavior.

The crystal-field Hamiltonian $\mathbf{H}_{\mathrm{CEF}}$ for the tetragonal symmetry D_{4h} of Pr^{3+} in Pr_2CuO_4 is given by

$$\mathbf{H}_{\mathrm{CEF}} = B_2^0 O_2^0 + B_4^0 O_4^0 + B_4^4 O_4^4 + B_6^0 O_6^0 + B_6^4 O_6^4 \qquad (1)$$

where the B_n^m denote the crystal-field parameters and the O_n^m's are operator equivalents built up by spin operators. Equation (1) gives rise to a decomposition of the ground-state J-multiplet $^3H_4$ of Pr^{3+} into five singlet states ($2\Gamma_1, \Gamma_2, \Gamma_3$ and Γ_4) and two doublet states ($2\Gamma_5$). The wave functions of the irreducible representations Γ_i are given by

$$|\Gamma_i\rangle = \sum_{M=-J}^{J} a_M^i |M\rangle \qquad (2)$$

from which we can readily derive the selection rules: we find that the crystal-field transitions $\Gamma_1 \to \Gamma_1$, $\Gamma_1 \to \Gamma_3$, $\Gamma_1 \to \Gamma_4$, $\Gamma_2 \to \Gamma_2$, $\Gamma_2 \to \Gamma_3$, $\Gamma_2 \to \Gamma_4$, $\Gamma_3 \to \Gamma_3$, $\Gamma_4 \to \Gamma_4$ are forbidden by symmetry arguments.

For the interpretation of the observed energy spectra we introduce the following parametrisation:

$$B_2^0 F_2 = W(1-|y|), \quad B_4^0 F_4 = W_{xy}, \quad B_6^0 F_6 = W(1-|x|)\,y, \qquad (3)$$

with $F_2 = 2$, $F_4 = 60$, $F_6 = 1260$; W is a scale factor. For the off-diagonal crystal-field parameters we use the relations

$$B_4^4 = -5.35\, B_4^0, \quad B_6^4 = 21.4\, B_6^0, \qquad (4)$$

which were determined from the quadratic-prismatic nearest-neighbor oxygen coordination surrounding Pr^{3+}. This procedure turned out to be an excellent approximation in recent studies [11] of the crystal-field interaction in $RBa_2Cu_3O_7$ compounds. With this in mind and considering the parameter range $-1 \leqq x \leqq 1$ and $-1 \leqq y \leqq 1$ we cover all possible combinations of second-, fourth- and sixth-order crystal-field parameters. For only one set of parameters x, y the energies and intensities of the observed crystal-field transitions turned out to be in agreement with the calculated values, namely for $x \approx 0.6$, $y \approx 0.4$ and $W > 0$. A refinement of the crystal-field parameters gave

$$B_2^0 = (1.6 \pm 0.1)\ \mathrm{meV},$$
$$B_4^0 = (2.7 \pm 0.2) \times 10^{-2}\ \mathrm{meV}, \qquad (5)$$
$$B_6^0 = (8.9 \pm 0.5) \times 10^{-4}\ \mathrm{meV}.$$

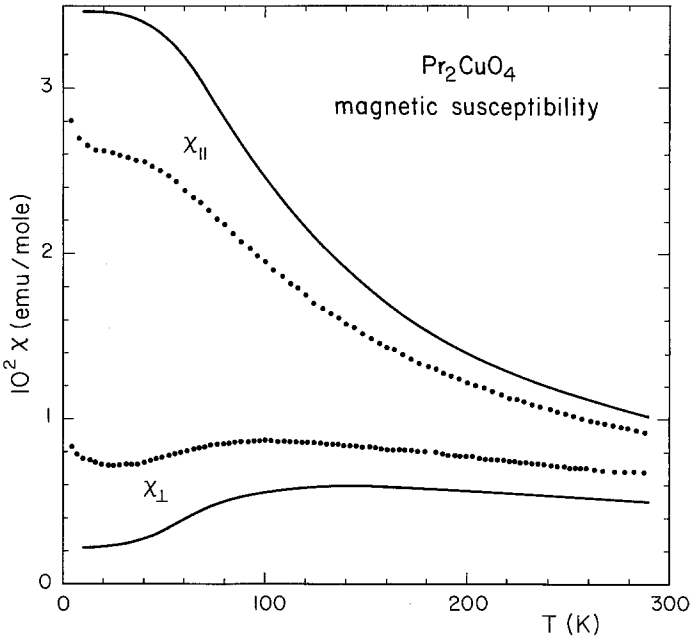

Fig. 7. Temperature dependence of the magnetic susceptibilities $\chi_{\parallel}$ (external field parallel to the basal plane) and $\chi_{\perp}$ (applied field perpendicular to the basal plane) for Pr_2CuO_4 measured on a single crystal from the same batch as used for our neutron diffraction work. The solid lines are calculated single-ion susceptibilities as obtained from the crystal-field parameters deduced in this work

The lower part of the resulting crystal-field level scheme is shown at the top of Fig. 6. Our model parameters predict the three highest crystal-field levels Γ_4, Γ_2, Γ_1 to lie at 147, 152, 181 meV, respectively; i.e. in an energy range not accessible in our INS experiments.

The crystal-field parameters (Eqs. 4 and 5) were used to calculate the magnetic properties of Pr_2CuO_4 associated with the Pr^{3+} ions. The magnetic single-ion susceptibility turns out to be highly anisotropic, yielding the x and y axes in the basal plane as the easy axes of magnetisation for the ionic Pr^{3+} moments. Our calculations are shown in Fig. 7 together with single-crystal data obtained in this work (see following section). From the crystal-field level scheme derived in the present study the Pr^{3+} ions are unlikely to order magnetically, since the ground state is a non-magnetic singlet state and the first-excited doublet is too far away in energy to induce any magnetic moment in the ground state.

3.4. *Macroscopic magnetisation*

Measurements of the macroscopic magnetisation were performed in a steady external magnetic field of 5 kOe as a function of temperature between liquid-helium and room temperature. The results are shown in Fig. 7 in the form of susceptibility plots for field directions parallel ($\chi_{\parallel}$) and perpendicular ($\chi_{\perp}$) to the Cu−O planes and they agree fairly well with previously published data [6]. The comparison with the calculated single-ion susceptibilities for Pr^{3+} mentioned above indicates that the temperature dependence and the anisotropy of χ are essentially determined by the magnetic properties of the rare-earth ions, but the absolute values of the susceptibility are clearly influenced by considerable exchange interactions. In particular we could not detect any sign for the onset of the Cu-ordering at 190 K in the $\chi(T)$ curves. A Curie-Weiss-like tail at lowest temperatures is most likely due to some free (Cu) moments; as the tail is more pronounced in $\chi_{\parallel}$ than in $\chi_{\perp}$ this effect does not seem to originate from rare-earth impurities.

Preliminary magnetisation measurements at fixed temperatures in fields up to 100 kOe indicate a possible field-induced phase transition involving the Cu moments as observed in La_2CuO_4 [10]; these data will be shown and discussed elsewhere.

4. Conclusions

From our study we conclude that the macroscopic magnetic properties of Pr_2CuO_4 can essentially be described by the magnetic single-ion response of Pr^{3+} and by additional exchange interactions. Microscopic measurements reveal antiferromagnetic ordering of the Cu-moments below 190 K in single crystals and below 250 K in powder material. Most features of this ordering, including the different ordering temperatures for single crystals and powder, are similar to those observed in La_2CuO_4 with the important exception of the temperature dependence of the Cu sublattice magnetisation. In view of the tendency to frustration in the given Cu sublattice it seems surprising that the transition temperatures are as high as 190 to 250 K, although no distinct structural changes in the T'-type phase could be detected. It is unlikely that the Pr^{3+} moments order at any temperature but it should be kept in mind that the exchange field due to the ordering of the Cu moments might have some influence on the magnetisation of the rare-earth ions, as observed recently in Gd_2CuO_4 [12].

Part of this work was financially supported by the Schweizerische Nationalfonds zur Förderung der wissenschaftlichen Forschung. Work at Los Alamos was done under the auspices of the US Department of Energy.

References

1. Akimitsu, J., Suzuki, S., Watanabe, M., Sawa, H.: J. J. Appl. Phys. **27**, L1859 (1988)
2. Tokura, Y., Takagi, H., Uchida, S.: Nature **337**, 345 (1989)
3. James, A.C.W.P., Zahurak, S.M., Murphy, D.W.: Nature **338**, 240 (1989)
4. Cheong, S.-W., Thompson, J.D., Fisk, Z.: Physica C**158**, 109 (1989)
5. Müller-Buschbaum, H., Wollschläger, W.: Z. Anorg. Allg. Chem. **414**, 76 (1975)
6. Hundley, M.F., Thompson, J.D., Cheong, S.-W., Fisk, Z., Oseroff, S.B.: Physica C**158**, 102 (1989)
7. Rietveld, H.M.: J. Appl. Crystallogr. **2**, 65 (1969); Hewat, A.W.: Report AERE-R7350, Atomic Energy Research Establishment, Harwell, Great Britain (1973)
8. Sears, V.F.: In: Methods of experimental physics. Vol. 23 (A): Neutron scattering. Sköld, K., Price, D.L. (eds.). New York: Academic 1986
9. Akimitsu, J., Ito, Y.: J. Phys. Soc. Jpn. **40**, 1621 (1976)
10. Birgeneau, R.J., Shirane, G.: Physical properties of High Temperature Superconductors. Ginsberg, D.M. (ed.). Singapore: World Scientific (1989, to be published)
11. Furrer, A., Brüesch, P., Unternährer, P.: Phys. Rev. B**38**, 4616 (1988)
12. Thompson, J.D., Cheong, S.-W., Brown, S.E., Fisk, Z., Oseroff, S.B., Tovar, M., Vier, D.C., Schultz, S.: Phys. Rev. B**39**, 6660 (1989)
13. Young, R.A., Prince, E., Sparks, R.A.: J. Appl. Crystallogr. **16**, 357 (1982)

P. Allenspach, P. Fischer, A. Furrer
Labor für Neutronenstreuung
Eidgenössische Technische Hochschule
Zürich
CH-5234 Villigen PSI
Switzerland

S.-W. Cheong, Z. Fisk
Los Alamos National Laboratory
Los Alamos, NM 87545
USA

A. Dommann
Laboratorium für Festkörperphysik
ETH Hönggerberg
CH-8093 Zürich
Switzerland

H.R. Ott
Laboratorium für Festkörperphysik
ETH Hönggerberg
CH-8093 Zürich
Switzerland

and

Paul Scherrer Institut
Labor für Festkörperforschung
CH-5234 Villigen PSI
Switzerland

B. Rupp
Paul Scherrer Institut
Labor für Festkörperforschung
CH-5234 Villigen PSI
Switzerland